International Communications in Heat and Mass
Transfer, 111, 104448, 2020

Compressible Fanno flows in micro-channels: an enhanced quasi-2D numerical model for turbulent flows

Marco Cavazzuti[1]*, Mauro A. Corticelli[1], Tassos G. Karayiannis[2]

[1]Dipartimento di Ingegneria "Enzo Ferrari", Università degli Studi di Modena e Reggio Emilia, via P. Vivarelli 10, 41125, Modena, Italy

[2]Department of Mechanical and Aerospace Engineering, Brunel University London, Uxbridge, Middlesex UB8 3PH, United Kingdom

Abstract

Fanno theory provides an analytical model for one-dimensional confined viscous compressible flows. The model holds under the assumptions of adiabatic flow and constant cross-section channel. From theory, the differential of every flow-related quantity is expressed as a function of Mach number and friction factor. One-dimensional flow numerical models can be derived by discretizing Fanno equations. However, theory does not assess how to evaluate friction, while the model works properly only if friction is estimated correctly. Compressibility and turbulence act by deforming the velocity profile making it flatter. Assuming the friction factor function of the Reynolds number alone, in line with incompressible flow theory, is thus not correct. Better correlations should include the Mach number to address compressibility effects. Here, the impact of turbulence and compressibility on the velocity profiles in a micro-channel is analysed by means of CFD simulations. Friction factor correlations are deduced for turbulent micro-flows. The impact of the velocity profile on other quantities, such as dynamic pressure and bulk temperature, needed for the numerical model operation, is also evaluated. Additional correlations for these quantities overcome the instrinsic limits of the one-dimensional model, necessarily unaware of local velocity profiles, in a quasi-2D fashion significantly improving its predicting capabilities.

Keywords

Compressible flow, Fanno flow, turbulent flow, micro-channels, friction factor

Highlights

- An enhanced model for solving turbulent Fanno flow in micro-channels is presented.
- Compressibility effects are investigated and addressed in a quasi-2D fashion.

*Corresponding author: Marco Cavazzuti, email: marco.cavazzuti@unimore.it, tel.: +39 059 2056347

- A detailed analysis of compressible velocity and temperature profiles is made.
- Correlations for dynamic pressure, bulk temperature, and friction are derived.
- The improved prediction capability of the numerical model is assessed.

Nomenclature

a	generic coefficient	P	cross-section perimeter	$\boldsymbol{\tau}$	stress tensor
A	cross-section area	$\dot{Q}$	thermal power	τ_{w}	wall shear stress
c	speed of sound	r	radial coordinate	ϕ	heat flux
c_{p}	heat capacity at constant pressure	R	channel radius	ω	turbulence specific dissipation rate
		R_{g}	specific gas constant		
D_{h}	hydraulic diameter	Re	Reynolds number		
E	total energy	T	temperature	*Subscripts*	
f	Darcy friction factor	U	velocity	0	upstream stagnation value
F_{v}	viscous forces resultant	x	longitudinal coordinate	1	downstream stagnation value
g	generic correction function	y	heightwise coordinate	avg	area-weighted average
h	specific enthalpy	y^+	dimensionless wall distance	blk	mass-weighted average
H	channel height			d	dynamic
k	turbulence kinetic energy	*Greek symbols*		e	effective
Kn	Knudsen number	α	length-to-diameter ratio	i	inlet section
L	channel length	γ	heat capacity ratio	o	outlet section
$\dot{m}$	mass flow rate	ϵ	surface roughness	s	Sutherland
Ma	Mach number	λ	thermal conductivity	t	total
n	normal-to-wall direction	μ	dynamic viscosity		
p	pressure	ρ	density		

1 Introduction

Recently, micro-scale fluid flow is attracting a growing interest thanks to miniaturization in many technological fields. Primarily, this is true in electronics where miniaturization is leading to very high dissipated power densities in many devices that require efficient micro-scale fluid cooling systems. Not limited to this, several applications are also found in the fields of refrigeration systems, heat pumps, pumps, reactors, turbomachinery, heat exchangers, aerospace engineering, to cite a few.

For instance, in [1] two-phase flow of R134a in capillary tubes was investigated experimentally and numerically for a refrigeration application, while in [2] the capillary flow of CO_2 for a transcritical heat pump cycle was studied analytically, observing that for a given capillary tube an optimum cooling capacity exists. In [3] the rapid depressurization in the micro-flow of supercritical fluids for an advanced sodium reactor application was analysed, while in [4] the flow in the blow-off lines of a heavy duty gas turbine was modelled using the Fanno theory.

Besides the numerous applications, other works investigate the problem from a more theoretical or analytical point of view as the understanding of the fundamental physics behind micro-scale fluid

flow and heat transfer still represents a challenge for the scientific community with regard to many aspects including multi-phase flows, boiling flows, rarefied gas condition, heat transfer, friction, and compressibility effects, either under laminar or turbulent flow condition.

For instance, in [5] a novel formulation was proposed for the prediction of compressible multi-phase flow in micro-channels, while boiling flow instabilities were investigated experimentally in [6] where flow pattern sequences were analyzed in detail. Unfortunately, with regard to compressibility effects, the literature is rather sparse. Some works can be found for the case of laminar adiabatic flow at intermediate Mach numbers, but the literature gets even sparser for turbulent, or diabatic, or higher Mach number flows. Laminar compressible single phase heat transfer was investigated analytically in [7]. An extensive review of single phase heat transfer was presented in [8]. Compressible friction factors in micro-channels were investigated in [9, 10] where laminar and turbulent correlations were proposed, respectively. The latter, though, proposes a correlation characterized by a singularity at $\mathrm{Ma} = 1$ resulting in infinite friction factor, so that it can only be applied with confidence to intermediate values of the Mach number. Other turbulent flow data from literature were presented in [11, 12] where equations are proposed for computing the average friction factor. The study of the rarefied gas flow condition is also attracting quite a lot of interest. When the Knudsen number is high enough, *e.g.* $10^{-3} \leq \mathrm{Kn} \leq 10^{-1}$, for instance due to gas rarefaction or to very small hydraulic diameters, the continuum hypothesis starts to break down and the flow is better modelled numerically by imposing a certain degree of tagential slip velocity and a temperature jump at the boundary wall. Different types of slip boundary conditions were discussed and compared in [13], while in [14] the temperature jump boundary condition was investigated for the case of turbulent flow. Other works focus on friction factor [15] and heat transfer characteristics [16, 17] in the slip flow regime.

The experimental study of compressible micro-flows poses a number of problems [18] primarily due to the difficulty in having a strict control over the channel dimension and wall relative roughness at such small scales. Moreover, still due to the scale of the problem, measurements are particularly error prone. This is mostly evident for temperature [19] and is reflected into the quality of friction and heat transfer predictions that can be made. The numerical approach is deemed more informative as it allows a much higher level of detail to be reached, and has been preferred in the current work, also with the support of analytical considerations.

Rather than inertia, micro-flows are dominated by surface friction [20] inducing large pressure drops in the fluid. When the fluid involved is a gas, this translates into abrupt accelerations and large velocities so that the fluid compressibility cannot be neglected.

Theoretical models for the analysis of compressible flow in channels were developed by Fanno and Rayleigh [21] in the early 20^{th} century. The two models were derived for constant-cross section channels, the former assuming non-isoentropic adiabatic flows, the latter isoentropic diabatic flow. The models are based on three first-order differential equations (conservation of mass, momentum, and energy), and allow the closed form prediction of the flow characteristics at any point along the channel once the boundary conditions, friction factor, and Mach number at one location are known. The more general case of non-isentropic diabatic flow cannot be solved in closed form but only numerically. Yet, due to

the effects induced by compressibility on the flow, friction is not constant and cannot be accurately estimated by the canonical fluid dynamic correlations (*e.g.* Colebrook-White and Blasius) as these hold only for incompressible flows. It has been shown [19, 22] that compressibility tends to flatten the velocity profile and as such it changes the velocity gradient at the wall, which is proportional to friction. A similar effect is induced by turbulence. The flattening of the profile also affects the dynamic pressure and temperature, and this must be taken into account for an accurate prediction of the flow characteristics.

In the present work an improved one-dimensional turbulent compressible Fanno flow numerical model is presented. The Fanno equations are solved on a fine grid so that changes in friction can be followed more closely, thus improving the quality of the solution. The model implements compressible correlations for the evaluation of friction and the assessment of dynamic pressure and temperature at each section as functions of Reynolds and Mach numbers. The correlations are derived from a detailed analysis of the velocity profiles from a set of CFD simulations. As such they are able to include additional information that normally would not be available in a one-dimensional model where at each section every flow characteristic is represented by a single average value. This gives the model a quasi-2D accuracy, making it more reliable than ordinary models that can be derived from the Fanno theory.

In a previous work [22], to which we refer for a more extensive treatment, the authors presented a similar analysis for the laminar case. There, the velocity profile was not affected by turbulence, and the correlations, given in terms of Poiseuille number for what concerns friction, were functions of the Mach number alone. Here the superposition of compressibility and turbulence effects on the shape of the velocity profiles is more complicated and nonlinear, requiring more elaborated correlations to be modelled.

2 Theoretical background

The main equations, at the basis of the Fanno theory and of the model proposed are briefly recalled here. For a more extensive treatment the reader is forwarded to [23], or to specialised textbooks [24].

First of all the definitions of speed of sound for an ideal gas and of Mach number are reminded

$$c = \sqrt{\gamma R_{\mathrm{g}} T}\,, \tag{1}$$

$$\mathrm{Ma} = \frac{U}{c}\,. \tag{2}$$

Then, the ideal gas law serves as a constitutive equation for the Fanno problem

$$p = \rho R_{\mathrm{g}} T\,. \tag{3}$$

The conservation equations (mass, momentum, and energy) are written as

$$\dot{m} = \rho U A\,, \tag{4}$$

$$\Delta\left(p + \rho U^2\right) = \frac{F_{\mathrm{v}}}{A}\,, \tag{5}$$

$$c_{\mathrm{p}}T + \frac{U^2}{2} = h_0\,. \tag{6}$$

These equations differ from the general isentropic case commonly found in textbooks for the assumption of a constant cross-section A and for the addition of the viscous forces resultant term in the momentum equation (Eq. (5))

$$F_{\mathrm{v}} = -\int P\tau_{\mathrm{w}}\,\mathrm{d}x = -\int \frac{Pf\rho U^2}{8}\,\mathrm{d}x\,, \tag{7}$$

which otherwise would read

$$p + \rho U^2 = p_0\,. \tag{8}$$

Similarly the Rayleigh theory, while adopting Eq. (8) for the momentum, adds a heat transfer term in the energy conservation equation so that it becomes

$$\Delta\left(c_{\mathrm{p}}T + \frac{U^2}{2}\right) = \frac{\dot{Q}}{\dot{m}}\,, \tag{9}$$

where

$$\dot{Q} = \int P\phi\,\mathrm{d}x = -\int P\lambda\frac{\partial T}{\partial n}\,\mathrm{d}x\,. \tag{10}$$

The parallelism between the two formulations is evident and it is interesting to note how friction for Fanno and heat for Rayleigh have the same effect of altering the density, and thus the velocity, of the fluid, eventually up to $\mathrm{Ma} = 1$ at the channel outlet section. This is achieved either by pressure drop due to friction (Fanno flow) or temperature rise due to heating (Rayleigh flow).

Considering the Fanno flow, with a few algebraic steps Eqs. (1)–(6) can be written in differential form of the main flow characteristic quantities as functions of Mach number and friction factor:

$$\begin{cases} \dfrac{\mathrm{d}p}{p} = \dfrac{-\gamma\mathrm{Ma}^2\left(1+(\gamma-1)\,\mathrm{Ma}^2\right)}{2\left(1-\mathrm{Ma}^2\right)}\dfrac{f\mathrm{d}x}{D_{\mathrm{h}}} \\ \dfrac{\mathrm{d}T}{T} = \dfrac{-\gamma\,(\gamma-1)\,\mathrm{Ma}^4}{2\left(1-\mathrm{Ma}^2\right)}\dfrac{f\mathrm{d}x}{D_{\mathrm{h}}} \\ \dfrac{\mathrm{d}U}{U} = -\dfrac{\mathrm{d}\rho}{\rho} = \dfrac{\gamma\mathrm{Ma}^2}{2\left(1-\mathrm{Ma}^2\right)}\dfrac{f\mathrm{d}x}{D_{\mathrm{h}}} \\ \dfrac{\mathrm{dMa}}{\mathrm{Ma}} = \dfrac{\gamma\mathrm{Ma}^2\left(1+\frac{\gamma-1}{2}\mathrm{Ma}^2\right)}{2\left(1-\mathrm{Ma}^2\right)}\dfrac{f\mathrm{d}x}{D_{\mathrm{h}}}\,, \end{cases} \tag{11}$$

where

$$f = -\frac{2D_{\mathrm{h}}\,\mathrm{d}p/\mathrm{d}x}{\rho U^2} = \frac{8\tau_{\mathrm{w}}}{\rho U^2} \tag{12}$$

is the Darcy friction factor. All the differentials in Eq. (11) change sign at $\mathrm{Ma} = 1$ marking a clear change in the fluid behaviour between subsonic and supersonic flow as expected. Similar conclusions could be drawn for Rayleigh flow.

3 Numerical model

A one-dimensional numerical model solving Fanno flow in micro-channels has been created. The channel is discretized in a number of segments where the governing equation are solved sequentially with an

explicit forward first-order Euler method. This has been deemed sufficient, also considering that the solution is quick, requiring only a few seconds of CPU time on an ordinary PC to solve a channel with a discretization as fine as 10^4 elements.

Considering that friction is not constant along the channel and all the expressions in Eq. (11) depend explicitly on friction and in order to avoid error superposition, it is preferred not to solve the governing equations in that form, except for the Mach number differential given below as Eq. (13).

$$\frac{\mathrm{dMa}}{\mathrm{Ma}} = \frac{\gamma \mathrm{Ma}^2 \left(1 + \frac{\gamma-1}{2}\mathrm{Ma}^2\right)}{2\left(1 - \mathrm{Ma}^2\right)} \frac{f \mathrm{d}x}{D_\mathrm{h}} \,, \tag{13}$$

The Mach number thus found is used to compute the remaining flow characteristic quantities resorting to Eqs. (1)–(6).

The boundary conditions needed are the stagnation temperature which is conserved across the channel $T_0 = T_1$, and the stagnation pressures upstream p_0 and downstream p_1 of the channel .

Due to the nature of Eq. (13) that returns a Mach number differential as function of Mach number itself, the governing equations can only be solved if the Mach number is known at some point along the channel. Since this is not the case a shooting technique is used in which a Mach number at the channel inlet $\mathrm{Ma_i}$ is guessed and the channel is solved up to when, for the given upstream boundary conditions, either the downstream pressure boundary condition is met or the sonic velocity is reached at the outlet section in agreement with the theory. Tolerances are given as stopping criteria for terminating the iterative search, namely:

$$\left|p_{\mathrm{t,o}} - p_1\right| \leq 0.1\,\mathrm{Pa}\,, \qquad 1 - \mathrm{Ma_o} \leq 10^{-5}\,. \tag{14}$$

As static temperature can drop quite significantly when Mach number grows, it is preferred to evaluate the thermophysical properties of the gas as function of temperature. For dynamic viscosity the two-coefficients Sutherland law is adopted

$$\mu = \frac{a_\mathrm{s}\sqrt{T}}{1 + T_\mathrm{s}/T} \,, \tag{15}$$

while for heat capacity JANAF coefficients are employed

$$c_\mathrm{p} = R_\mathrm{g} \sum_{i=0}^{4} a_i T^i \,. \tag{16}$$

The Reynolds number, needed for computing friction factor, is evaluated as

$$\mathrm{Re} = \frac{\rho U D_\mathrm{h}}{\mu} = \frac{\dot{m} D_\mathrm{h}}{\mu A} \,, \tag{17}$$

while the Knudsen number, needed to check whether the continuum hypothesis with no slip wall and no temperature jump boundary conditions is acceptable, is computed for a gas as

$$\mathrm{Kn} = \frac{\mathrm{Ma}}{\mathrm{Re}} \sqrt{\frac{\gamma\pi}{2}} \,. \tag{18}$$

The quality of one-dimensional Fanno flow model predictions depends upon a few quantities that must be carefully addressed, such as friction, dynamic pressure, and dynamic temperature.

As friction enters directly in Eq. (13) it is important that this quantity is evaluated correctly to avoid error propagation to the Mach number and to all other quantities. In case of incompressible flow, friction is known to depend upon Reynolds number, and if the channel walls are not sufficiently smooth also on relative roughness. Yet compressibility, by altering the velocity profiles, also affects friction and this must be taken into account with proper correlations for the compressible flow case.

The governing equations allow static pressure to be computed in each element. Yet, the pressure stopping criterion in Eq. (14) is given in terms of total pressure $p_\mathrm{t} = p + p_\mathrm{d}$. The accurate evaluation of dynamic pressure becomes thus important so that the shooting technique will stop when the correct guess of the inlet Mach number is made. Locally the value of dynamic pressure is $p_\mathrm{d} = \rho U^2/2$ but when this is integrated over the cross-section the average velocity and density values available from Fanno equations are not sufficient for an accurate prediction of the dynamic pressure

$$p_{\mathrm{d,avg}} = \frac{\int_A \frac{\rho U^2}{2}\,\mathrm{d}A}{\int_A \mathrm{d}A} \neq \frac{\rho_\mathrm{blk} U_\mathrm{avg}^2}{2}\,. \tag{19}$$

From the analysis of compressible velocity profiles and their integration, a proper function g can be derived so that dynamic pressure can be accounted for in the Fanno model using the average known quantities

$$p_{\mathrm{d,avg}} = g\frac{\rho_\mathrm{blk} U_\mathrm{avg}^2}{2}\,. \tag{20}$$

Finally, an accurate prediction of temperature is needed for the correct evaluation of fluid thermophysical properties, including speed of sound, density, heat capacity, and viscosity. Similarly, from Eq. (6) it is known that total temperature is conserved but its dynamic component varies with velocity, *i.e.* $T_\mathrm{t} = T + T_\mathrm{d}$. Thus, the same considerations raised for pressure hold also here. Locally the dynamic temperature is defined as $T_\mathrm{d} = U^2/2c_\mathrm{p}$, but integrating over the cross-section, the average velocity and heat capacity are not sufficient for its prediction, *i.e.*

$$T_{\mathrm{d,blk}} = \frac{\int_A \rho U \frac{U^2}{2c_\mathrm{p}}\,\mathrm{d}A}{\int_A \rho U\,\mathrm{d}A} \neq \frac{U_\mathrm{avg}^2}{2c_{\mathrm{p,blk}}}\,. \tag{21}$$

From the integration of compressible velocity profiles, a proper function g can be found so that

$$T_{\mathrm{d,blk}} = g\frac{U_\mathrm{avg}^2}{2c_{\mathrm{p,blk}}}\,. \tag{22}$$

We refer to the g functions by calling them correction functions, intending that they operate as corrections that, applied to the gross formulae computed on the basis of the average quantities, make them accurate.

The present work discusses and proposes correlations for the evaluation of friction, dynamic pressure, and dynamic temperature so that the accuracy of the one-dimensional Fanno numerical model could be improved.

4 Simulations setup

The correlations for f, $p_{\mathrm{d,avg}}$, and $T_{\mathrm{d,blk}}$, come from a detailed analysis of turbulent compressible velocity profiles in smooth micro-channels after a set of CFD results. Overall 52 simulations were performed,

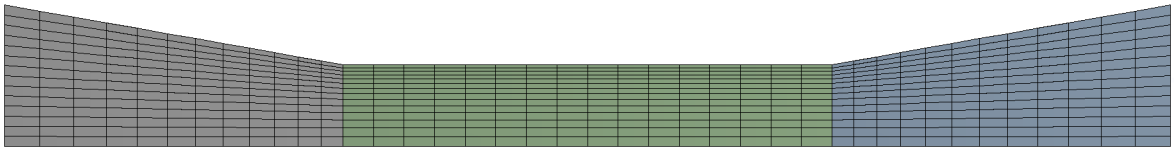

Figure 1: Off-scale mesh example.

chosen to span Mach numbers in the subsonic region (inlet Mach number is always < 1) and Reynolds numbers in transient and turbulent regions from 3 000 to 20 000. Two channel cross-section types are considered (circular and parallel-plate), for two channel length-to-diameter ratios ($\alpha = 100$ and $\alpha = 500$), and two stagnation temperatures ($T_0 = 300\,\mathrm{K}$ and $T_0 = 500\,\mathrm{K}$). For each permutation of these three parameters a series of simulations was performed for growing upstream stagnation pressures p_0 up to when the sonic condition is met at the outlet ($\mathrm{Ma_o} = 1$), while the downstream stagnation pressure p_1 is kept at 1 bar. The hydraulic diameter of the channel D_h is fixed at 0.5 mm.

The Ansys Fluent code is used for the simulations as it provides a stable coupled solver, needed for the convergence of highly compressible flows. The mesh is either axisymmetric or planar depending on the channel cross-section type, fully structured, with maximum $y^+ < 0.5$. Plenums are added at the channel ends gradually expanding the cross-section up to when its area becomes at least 400 times that of the channel. In this way inlet and outlet pressure boundary conditions are imposed in regions where $p_\mathrm{t} \approx p$. Depending on the fluid velocity and the boundary conditions, the y^+ target requires different mesh sizes to be employed ranging from 250 thousand to 5 million elements. A 500 elements off-scale mesh example is shown in Fig. 1. Boundary conditions are total pressure imposed at the inlet (boundary on the left), static pressure at the outlet (boundary on the right), no-slip wall at the upper boundary, and either axial symmetry or symmetry plane on the bottom boundary depending on the cross-section type. Second-order discretization schemes are used together with SST k-ω turbulence model. The set of equations solved is the following

$$\begin{cases} \nabla \cdot (\rho \mathbf{U}) = 0 & \text{Mass conservation} \\ \nabla \cdot (\rho \mathbf{U}\mathbf{U}) = -\nabla p + \nabla \cdot \boldsymbol{\tau} & \text{Momentum conservation} \\ \nabla \cdot (\rho \mathbf{U}\,(E + p/\rho)) = \nabla \cdot (\lambda_\mathrm{e} \nabla T + \boldsymbol{\tau} \cdot \mathbf{U}) & \text{Energy conservation} \\ \nabla \cdot (\rho \mathbf{U} k) = \nabla \cdot (\Gamma_\mathrm{k} \nabla k) + G_\mathrm{k} - Y_\mathrm{k} & \text{Transport of } k \\ \nabla \cdot (\rho \mathbf{U} \omega) = \nabla \cdot (\Gamma_\omega \nabla \omega) + G_\omega - Y_\omega + Z_\omega & \text{Transport of } \omega \end{cases} \tag{23}$$

where $\boldsymbol{\tau} \cdot \mathbf{U}$ is the viscous heating term, and in the last two transport equations Γ represents the effective diffusivity, G the production, Y the dissipation, and Z the cross-diffusion terms. The solution convergence is pushed to maximum residuals $< 10^{-8}$ for every equation solved.

Figure 2 shows the results of the grid independence test. Conservatively, the study has been performed on a high Mach number case where the effects of compressibility are stronger and errors tend to be larger compared to other cases. In the figure the $y^+ = 0$ value, which would require an infinitely fine mesh, is predicted using Richardson extrapolation [25]

$$f_{y^+=0} = f_n + \frac{f_n - f_{n-1}}{\left(y^+_{n-1}/y^+_n\right)^2 - 1}\,, \tag{24}$$

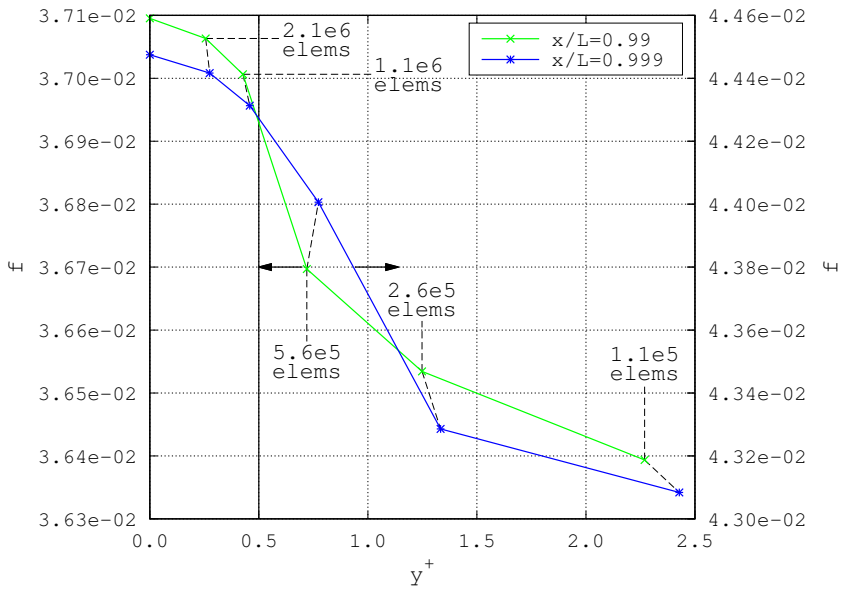

Figure 2: Grid independence test: friction predicted at two longitudinal coordinates close to the channel outlet with mesh of different refinements. The figure refers to the circular cross-section case with $\alpha = 500$, $T_0 = 300\,\mathrm{K}$, $p_0 = 4.6\,\mathrm{bar}$. The vertical line shows the y^+ constraint, arrows indicate the reference coordinate axis for each line.

where the n subscript stands for the solution corresponding to the finest mesh available and $n-1$ to the second finest mesh. The y^+ constraint applied for mesh acceptance and marked by the vertical line in the figure allows to estimate a maximum error in the prediction of friction $\approx 0.5\%$.

During the simulations post-processing information on static and total pressure, static and total temperature, velocity, velocity profile, Mach number, wall shear stress, and on the fluid thermophysical properties are extracted at 65 sections along the channel. The sections distribution is non-uniform and is finer close to the channel outlet where gradients are larger. Reported Knudsen numbers are always $< 2 \times 10^{-4}$.

5 Velocity profiles

5.1 Velocity profiles evolution

Figure 3 shows the typical velocity profile and friction factor evolution in a turbulent micro-channel from inlet to outlet. The figure refers to a choked flow case so that compressibility effects can be better appreciated as Mach number approaches unity.

At the channel inlet the velocity profile is rather flat (Fig. 3a). A particularly high local friction factor corresponds to this (Fig. 3b). Then entrance effects start to fade and the velocity profile develops toward a parabolic shape remaining at first laminar (Fig. 3a) while friction drops significantly (Fig. 3b). Before a developed laminar profile can be reached the flow turns unstable and this brings a sudden change in the shape of the velocity profile (see the dash-dotted line in Fig. 3a) and also a rapid increase

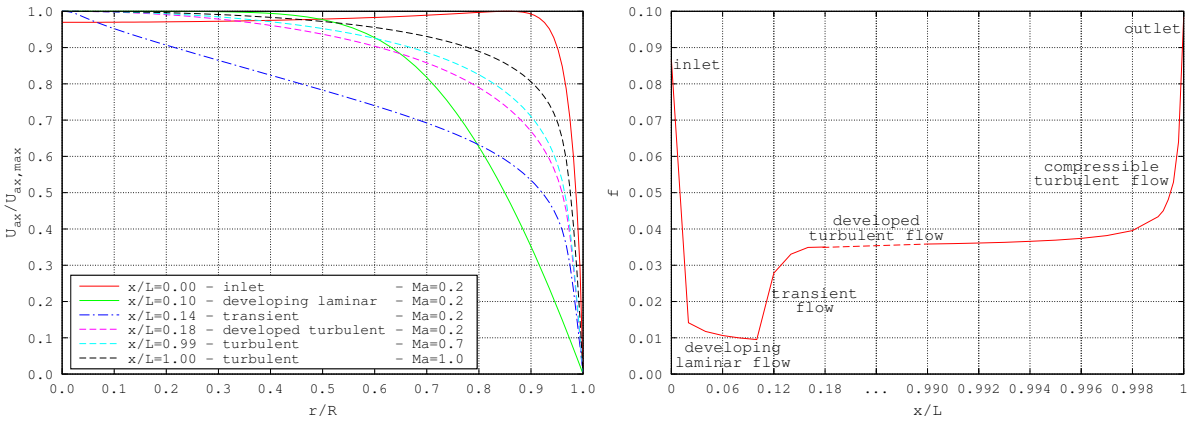

(a) Normalized axial velocity profiles

(b) Friction factor

Figure 3: Velocity profiles and friction factor evolution from channel inlet to outlet. The figure refers to the circular cross-section case with $\alpha = 500$, $T_0 = 300\,\mathrm{K}$, $p_0 = 4.6\,\mathrm{bar}$.

of friction factor (Fig. 3b). The flow is now turbulent and, unless the channel is particularly short, the Mach number still low. At this point a developed flow velocity profile is reached quickly and is maintained for most of the channel length (note the different scaling of the abscissa on the left and on the right portions of Fig. 3b). In this region Mach number grows imperceptibly. As a consequence the velocity profile remains essentially unchanged (Fig. 3a) and friction factor constant (Fig. 3b). The shape of the profile depends only on Reynolds number, being flatter for higher Reynolds numbers. The situation changes, and very suddenly, only close to the channel outlet. In just a few millimeters length the sonic flow condition ($\mathrm{Ma_o} = 1$) is reached and the velocity profile becomes particularly flat (Fig. 3a) while its shape is essentially a function of the Mach number with minor influences of the Reynolds number. Correspondingly, the friction factor grows exponentially (Fig. 3b). Even though the impact of compressibility is evident only on a very small portion of the channel length, the changes that occur in all the flow characteristic quantities are so large and sharp that the constant friction hypothesis, while mostly true, becomes insufficient for an accurate prediction of compressible flow in the micro-channel in its entirety. All the changes in the velocity profile presuppose a radial (or heightwise) mass transfer towards the channel centre as the flow develops, and away from the centre as compressibility becomes more evident.

5.2 Compressibility effects

Compressibility effects can be highlighted by analysing the velocity profiles and their dependency on Reynolds and Mach numbers.

Profiles along 65 sections are extracted from each of the 52 CFD simulations. The set of 3380 profiles is then cleared by those where entrance effects are still evident. With reference to Fig. 3b this means that all the samples before a developed turbulent flow condition is attained are removed. The cutoff point is never evident due to the flat gradient at the end of the transition region, and has been chosen after the inflection point of the friction interpolating curve.

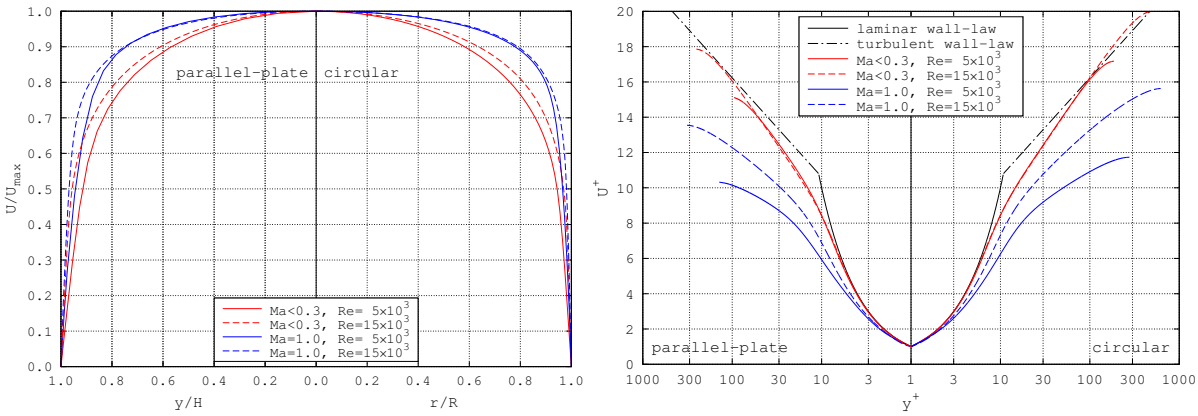

(a) Normalized axial velocity profiles

(b) Axial velocity profiles on the y^+–U^+ plane

Figure 4: Velocity profiles for different Reynolds and Mach numbers: parallel-plate vs circular cross section channel.

Similarly, samples at the outlet section show some minor offset in the axial trend of friction and other quantities, and are therefore removed. This reveals the presence of outlet effects where the flow is affected, even if marginally, by the cross-section expansion at the end of the channel. In line with this, average Mach numbers moderately larger than unity can also be found in the region as the flow is no longer constrained by the channel walls. This is discussed also in [26] where a thinning of the boundary layer and abrupt changes in friction are reported when the Mach number grows above unity. In the current CFD simulations the length of channel over which these outlet effects are evident is extremely limited and never exceeds $D_\mathrm{h}/5$. Even though this is apparently in contrast with Fanno theory, it must be reminded that the theory concern is in modelling what happens inside the channel and not across the channel outlet section towards the external ambient where other factors may influence the flow field.

Overall, 828 profiles are left for the circular and 843 for the parallel-plate cross-section cases. Some of the $\alpha = 100$ simulations had to be entirely discarded from the set since the channel was too short for allowing a developed turbulent flow region. The transition either did not occur or occurred too close to the channel outlet so that entrance, compressibility, and outlet effects could not be clearly separated.

By plotting the normalized velocity profiles it is clear that, for a given cross-section type, sections with the same Reynolds and Mach numbers are perfectly superimposable. The same could not be said by comparing the profiles in terms of other flow characteristics or their derivative. This was already found and discussed in some papers such as in [10].

Figure 4a shows a set of velocity profiles for the two cross-sections types considered, and two different Reynolds and Mach numbers. For each nondimensional group one small and one large value are chosen to better appreciate their impact on the profile shape. The profile gets flatter with increasing Reynolds and Mach numbers, the impact of Reynolds number being more evident at low Mach numbers, and *vice versa*. This simply means the margin for profile flattening is smaller when the profile is already flattened for some reason. The impact of Reynolds number is stronger for moderately turbulent flows and damps out as the Reynolds number is increased. On the contrary, the impact of Mach number is negligible for

incompressible flows and grows very strong for larger Mach number, making Reynolds number almost negligible close to $\mathrm{Ma} = 1$.

Comparing the two cross-section types in Fig. 4a it is noted that the profiles are flatter for the circular cross-section case, but the differences become less evident for larger Reynolds numbers.

In Fig. 4b the same profiles are plotted on the nondimensional y^+–U^+ plane. The turbulent low-Mach number profiles follow closely the law of the wall as expected, while the high-Mach number profiles depart from the wall law being shifted downwards for higher y^+ values, this is also a sign of flatter velocity profile.

6 Turbulent compressible flow correlations

As the velocity profile changes with Reynolds and Mach numbers, so friction and the g functions in Eq. (20) and in Eq. (22) do. Except g, all the terms in the equations are readily available from the CFD simulations, making it possible to map friction and g on each section in function of Reynolds and Mach numbers as follows

$$\begin{cases} f(\mathrm{Re},\mathrm{Ma}) = \dfrac{\tau_\mathrm{w}}{\rho_\mathrm{blk} U_\mathrm{avg}^2/8} \\ g_{p_\mathrm{d}}(\mathrm{Re},\mathrm{Ma}) = \dfrac{p_\mathrm{d,avg}}{\rho_\mathrm{blk} U_\mathrm{avg}^2/2} \\ g_{T_\mathrm{d}}(\mathrm{Re},\mathrm{Ma}) = \dfrac{c_\mathrm{p,blk} T_\mathrm{d,blk}}{U_\mathrm{avg}^2/2} \,. \end{cases} \tag{25}$$

Figure 5 shows the result of this operation, where CFD data is both plotted against Mach (on the left) and Reynolds numbers (on the right). Dynamic temperature plots are omitted for brevity, being similar to the dynamic pressure ones.

The figures on the left show clear trends for each simulation where friction (and the other quantities) are rather constant for low Mach number values, then change more and more rapidly as Mach number approaches unity. The trends are not superimposable since every simulation is characterized by different Reynolds numbers, and larger Reynolds numbers shift all data downward on the ordinate axis. Moreover, the deviation from the constant value is seen to occur at higher Mach numbers when Reynolds number is larger.

In the figures on the right trends are even clearer and data from each simulation is again discernible. In each set we can distinguish between low Mach number data where the values are moderately reduced for growing Reynolds numbers, and high Mach number data where the samples depart more and more rapidly from the previous trend (upward for friction, downward for pressure and temperature corrections) as the Mach number is increased. It is noted how incompressible data in Fig. 5b gradually tend to the well-known Blasius [27]

$$f = \frac{0.316}{\mathrm{Re}^{1/4}} \tag{26}$$

or the smooth pipe Colebrook-White [28]

$$\frac{1}{\sqrt{f}} = -2\log\left(\frac{2.51}{\mathrm{Re}\sqrt{f}}\right) \tag{27}$$

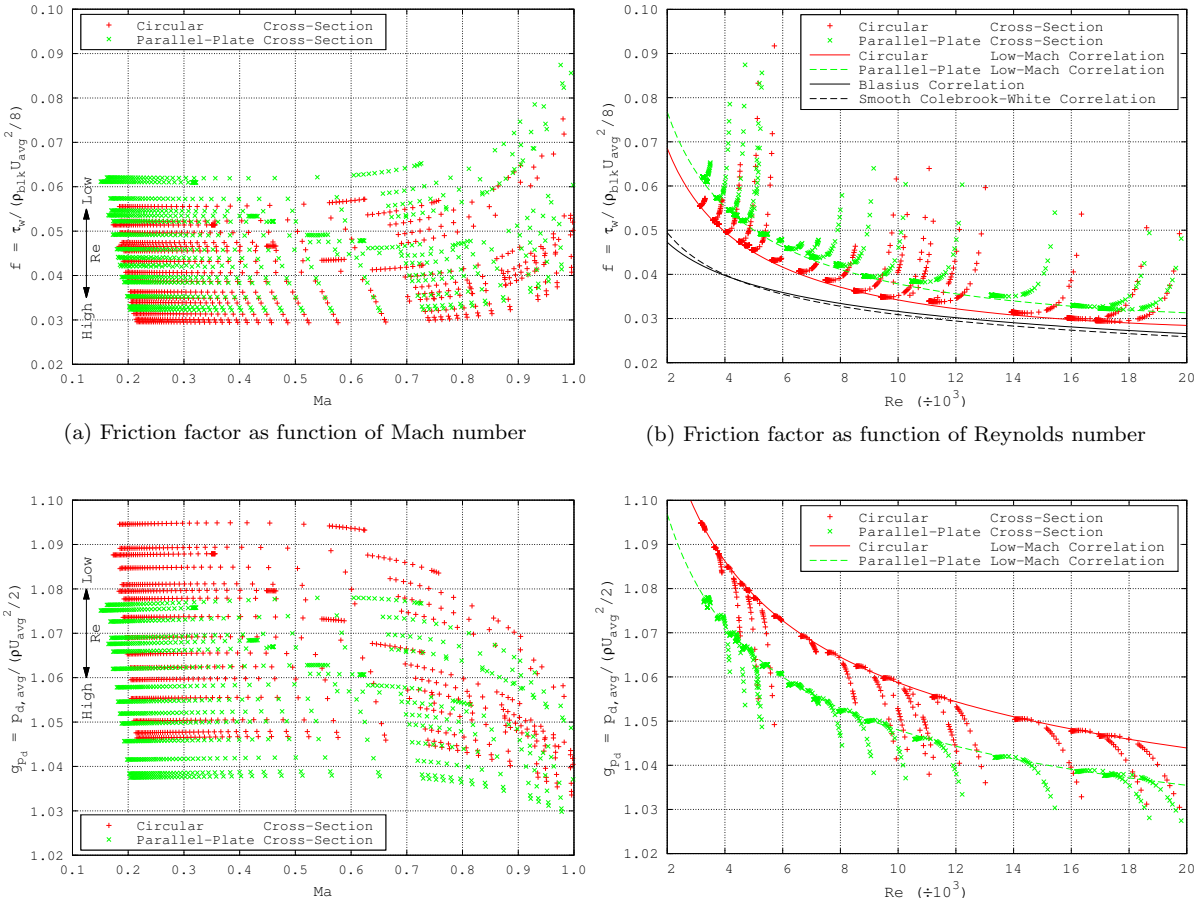

(a) Friction factor as function of Mach number

(b) Friction factor as function of Reynolds number

(c) Dynamic pressure correction as function of Mach number

(d) Dynamic pressure correction as function of Reynolds number

Figure 5: Turbulent compressible friction factor and dynamic pressure correction as function of Mach (left) and Reynolds numbers (right) for the set of 1671 eligible profiles.

correlations for incompressible flow as Reynolds number is increased and the flow becomes fully turbulent.

Overall this calls for rather complicated two-variable formulas for data to be correlated in which we can distinguish between a low-Mach number region where the correlations depend only on Reynolds number, and a high-Mach number region where both Reynolds and Mach numbers affect the solution, even though the latter dominates. There is no net distinction between these two regions as the passage is smooth and, as already noted, occurs at different Mach numbers for different Reynolds numbers.

In view of these considerations it has been opted for a two-step data interpolation in which a low-Mach number correlation is given first as function of Reynolds number, and is then expanded by multiplying it by a high-Mach number correlation function of Reynolds and Mach numbers.

Considering low-Mach number data in Fig. 5b, it is noted that the same decreasing trend of friction is seen for pressure and temperature corrections with the only difference that the former tends to zero for infinite Reynolds number and g functions to one. For this reason, correlations in the form of

Blasius formula, Eq. (26), are deemed good candidates for data interpolation. The low-Mach number correlations are thus chosen of the type:

$$\begin{cases} a_1 \mathrm{Re}^{a_2 + a_3 \mathrm{Re}} & \text{for friction factor} \\ 1 + a_1 \mathrm{Re}^{a_2} & \text{for dynamic pressure and temperature corrections,} \end{cases} \tag{28}$$

where a_1 is a positive number, and a_2 negative. A small positive a_3Re term has been added in friction correlation for better data interpolation. The evident curvature change between low and high-Reynolds number data in Fig. 5b would not have been achievable with a constant exponent in the exponential function.

For high-Mach number correlation a similar form has been chosen where both Mach and Reynolds numbers appear

$$1 + a_4 \mathrm{Ma}^{a_5} \mathrm{Re}^{a_6} \,. \tag{29}$$

From Fig. 5, positive a_4 values for friction, and negative for pressure and temperature corrections are expected. a_5 will be positive since larger gradients are always found for larger Mach numbers. Similarly a_6 will be negative since gradients are smaller for larger Reynolds numbers.

Overall, the generic correlation proposed has the form

$$a_0 + \left(a_1 \mathrm{Re}^{a_2 + a_3 \mathrm{Re}}\right)\left(1 + a_4 \mathrm{Ma}^{a_5} \mathrm{Re}^{a_6}\right) \tag{30}$$

with a_0 either zero or one. This is not the only possible equation form for correlating the set of data at hand, yet Eq. (30) is relatively simple, depends on a limited set of parameters, and provides good data interpolation as shown in the following.

6.1 Circular cross-section

The following correlations apply for the circular cross-section case. For friction factor

$$f\,(\mathrm{Re},\,\mathrm{Ma}) = \left(\frac{3.159}{\mathrm{Re}^{0.51 - 1.57 \cdot 10^{-6} \mathrm{Re}}}\right)\left(1 + 49.75\,\frac{\mathrm{Ma}^{9.22}}{\mathrm{Re}^{0.47}}\right) \tag{31}$$

is found with an average interpolation error of 1.99%, while for dynamic pressure and temperature corrections we have

$$g_{p_\mathrm{d}}\,(\mathrm{Re},\,\mathrm{Ma}) = 1 + \left(\frac{2.789}{\mathrm{Re}^{0.42}}\right)\left(1 - 0.658\,\frac{\mathrm{Ma}^{6.45}}{\mathrm{Re}^{0.103}}\right) \tag{32}$$

with an average interpolation error of 0.79%, and

$$g_{T_\mathrm{d}}\,(\mathrm{Re},\,\mathrm{Ma}) = 1 + \left(\frac{6.603}{\mathrm{Re}^{0.41}}\right)\left(1 - 1.230\,\frac{\mathrm{Ma}^{5.53}}{\mathrm{Re}^{0.141}}\right) \tag{33}$$

with an average interpolation error of 0.99%.

6.2 Parallel-plate cross-section

The following correlations apply for the parallel-plate cross-section case. For friction factor

$$f\,(\mathrm{Re},\,\mathrm{Ma}) = \left(\frac{3.744}{\mathrm{Re}^{0.51 - 1.57 \cdot 10^{-6} \mathrm{Re}}}\right)\left(1 + 82.58\,\frac{\mathrm{Ma}^{9.24}}{\mathrm{Re}^{0.53}}\right) \tag{34}$$

Table 1: Synoptic table of the correlation coefficients following the form in Eq. (30).

Correlation	Cross-section	a_0	a_1	a_2	a_3 ($\times 10^6$)	a_4	a_5	a_6	Average Error
f	Circular	0	3.159	−0.51	1.57	49.75	9.22	−0.47	1.99%
g_{p_d}	Circular	1	2.789	−0.42	0	−0.658	6.45	−0.103	0.79%
g_{T_d}	Circular	1	6.603	−0.41	0	−1.230	5.53	−0.141	0.99%
f	Parallel-plate	0	3.744	−0.51	1.57	82.58	9.24	−0.53	1.80%
g_{p_d}	Parallel-plate	1	2.672	−0.44	0	−0.276	8.91	−0.028	1.51%
g_{T_d}	Parallel-plate	1	5.591	−0.42	0	−2.188	7.84	−0.223	0.96%

is found with an average interpolation error of 1.80%, while for dynamic pressure and temperature corrections we have

$$g_{p_\mathrm{d}}\left(\mathrm{Re},\,\mathrm{Ma}\right) = 1 + \left(\frac{2.672}{\mathrm{Re}^{0.44}}\right)\left(1 - 0.276\,\frac{\mathrm{Ma}^{8.91}}{\mathrm{Re}^{0.028}}\right) \tag{35}$$

with an average interpolation error of 1.51%, and

$$g_{T_\mathrm{d}}\left(\mathrm{Re},\,\mathrm{Ma}\right) = 1 + \left(\frac{5.591}{\mathrm{Re}^{0.42}}\right)\left(1 - 2.188\,\frac{\mathrm{Ma}^{7.84}}{\mathrm{Re}^{0.223}}\right) \tag{36}$$

with an average interpolation error of 0.96%.

The six correlations are composed by a low-Mach number term function of Reynolds number (first parenthesis) and a high-Mach number term function of Reynolds and Mach numbers (second parenthesis). The low-Mach number term is also plotted in Fig. 5 (figures on the right), showing the accuracy of the interpolation.

Table 1 resumes the coefficients and the accuracy of all the correlations proposed, while Fig. 6 shows three-dimensional plots of the correlations with the superposition of CFD data from the 1671 sections. The very good match between the correlations and the numerical data is evident. Finally, friction correlations in Eq. (31) and in Eq. (34) are plotted on a Moody's chart for different Mach numbers in Fig. 7. The compressible predictions of course are inherent to smooth channels as roughness is not addressed in the current work. It is reminded that the correlations are suited for $0 \leq \mathrm{Ma} \leq 1$ and $3\,000 \leq \mathrm{Re} \leq 20\,000$.

7 Results

For validation purposes, the enhanced one-dimensional model implementing the correlations in Eqs. (31)–(36) is tested against additional simulations having different geometry and boundary conditions compared to those used for calibrating the correlations. The improved prediction capabilities over the standard Fanno model is tested for two extreme cases reaching the sonic flow condition at the channel outlet so that both the correlation terms can be tried. With the term standard model we refer to the one-dimensional model that can be derived from Fanno theory in which friction is computed with the

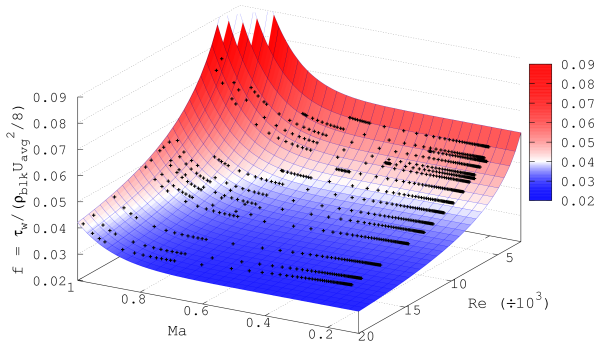

(a) Friction factor correlation, circular cross-section case, Eq. (31)

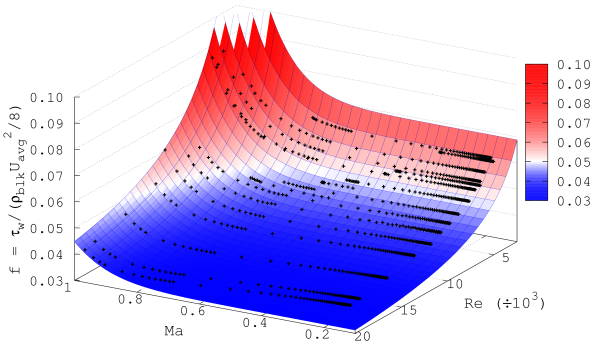

(b) Friction factor correlation, parallel-plate cross-section case, Eq. (34)

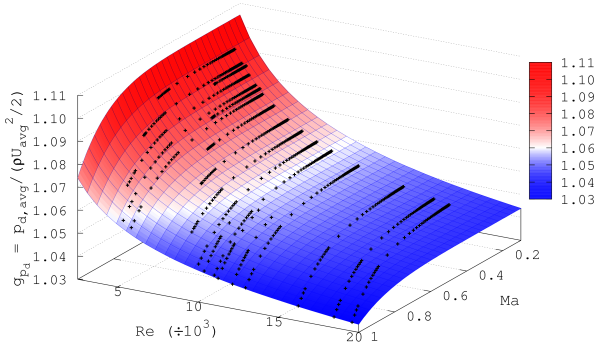

(c) Dynamic pressure correction correlation, circular cross-section case, Eq. (32)

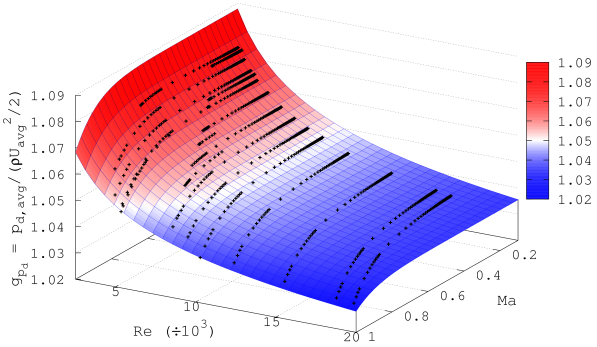

(d) Dynamic pressure correction correlation, parallel-plate cross-section case, Eq. (35)

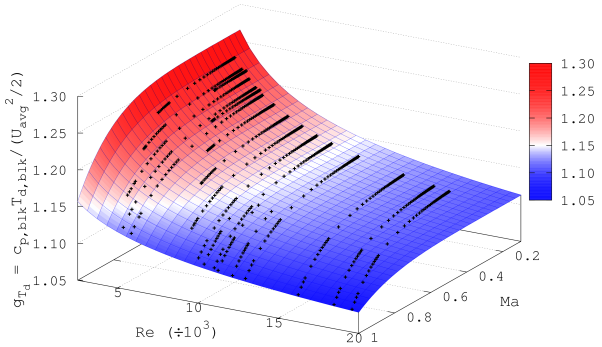

(e) Dynamic temperature correction correlation, circular cross-section case, Eq. (33)

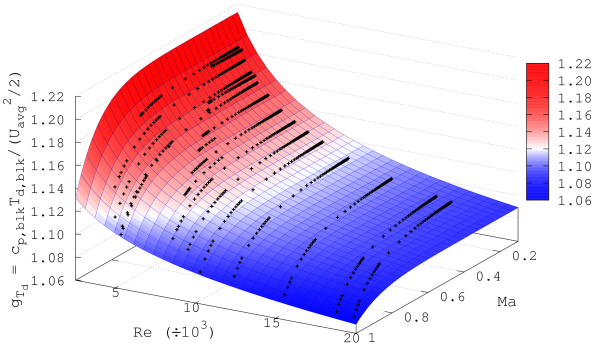

(f) Dynamic temperature correction correlation, parallel-plate cross-section case, Eq. (36)

Figure 6: Three-dimensional plots of the correlations in Eqs. (31)-(36) (coloured surfaces) with the superposition of data relative to the 1671 sections from CFD simulations (small + signs).

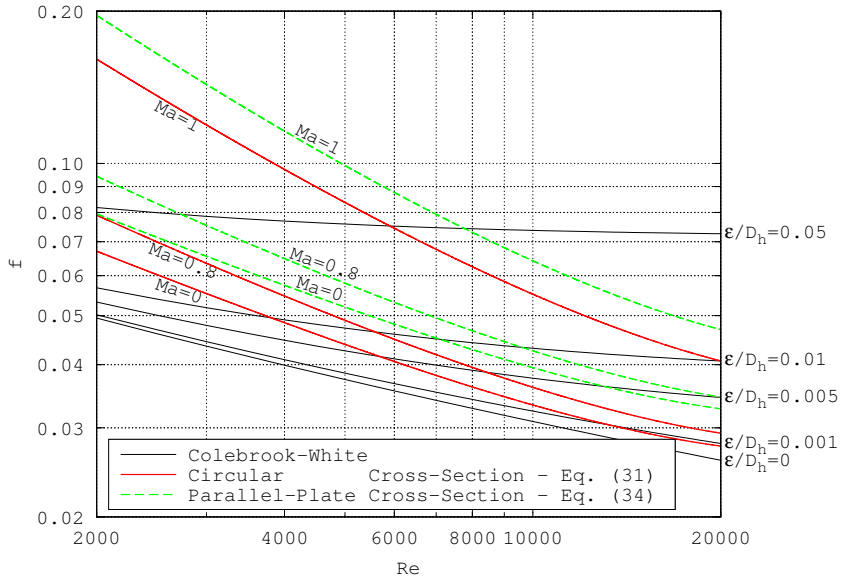

Figure 7: Friction factor correlations plotted against Colebrook-White equation for different relative roughness values on Moody's chart.

Blasius formula and pressure and temperature corrections are not implemented.

The first simulation refers to a low Reynolds number case (Re $\approx 4\,000$): a region where gradients are high and correction terms far from unity. Here the correlation interpolation errors are higher than average. Namely this simulation refers to the parallel-plate cross-section case with $\alpha = 1\,000$, $D_\mathrm{h} = 0.4\,\mathrm{mm}$, $T_0 = 300\,\mathrm{K}$, $p_0 = 9.0\,\mathrm{bar}$, $p_1 = 1.0\,\mathrm{bar}$.

The second simulation refers to a case where Reynolds number is way beyond the correlations range of validity (Re $\approx 50\,000$). Such a high Reynolds number is unusual in micro-channels: rather than having a practical interest, this simulation aims at testing the model in an uncommon environment where the correlations proposed need to be extrapolated. In this region friction factor is well approximated by Blasius formula and the correction terms tend to one. This means that the enhanced model tends to the standard one so that differences between the two should be marginal. It must be noted that while dynamic pressure and temperature formulae are consistent and could be extrapolated safely beyond Re $= 20\,000$ since they are monotonic and fade to one for growing Reynolds numbers, the same could not be said for friction. The addition of the $a_3\mathrm{Re}$ term in Eq. (31) and in Eq. (34) makes the low-Mach number portion of the correlation non-monotonic with respect to Reynolds number (with a minimum close to Re $= 29\,000$), and thus unsuitable for extrapolation. For avoiding any bias in the comparison, the low-Mach number term in friction factor correlations has been substituted with the Blasius formula. The simulation used for this validation refers to the circular cross-section case with $\alpha = 1\,000$, $D_\mathrm{h} = 2.0\,\mathrm{mm}$, $T_0 = 600\,\mathrm{K}$, $p_0 = 6.0\,\mathrm{bar}$, $p_1 = 1.0\,\mathrm{bar}$.

Since entrance effects are not addressed in the current work, for a more fair comparison the entrance region is skipped: this is achieved by reading the total pressure at $x = 100 D_\mathrm{h}$ in the CFD simulations and imposing it as upstream boundary condition of a $\alpha = 900$ channel solved with the one-dimensional model. The results of the validation are shown in Fig. 8. Note the different abscissa range in Figs. 8a

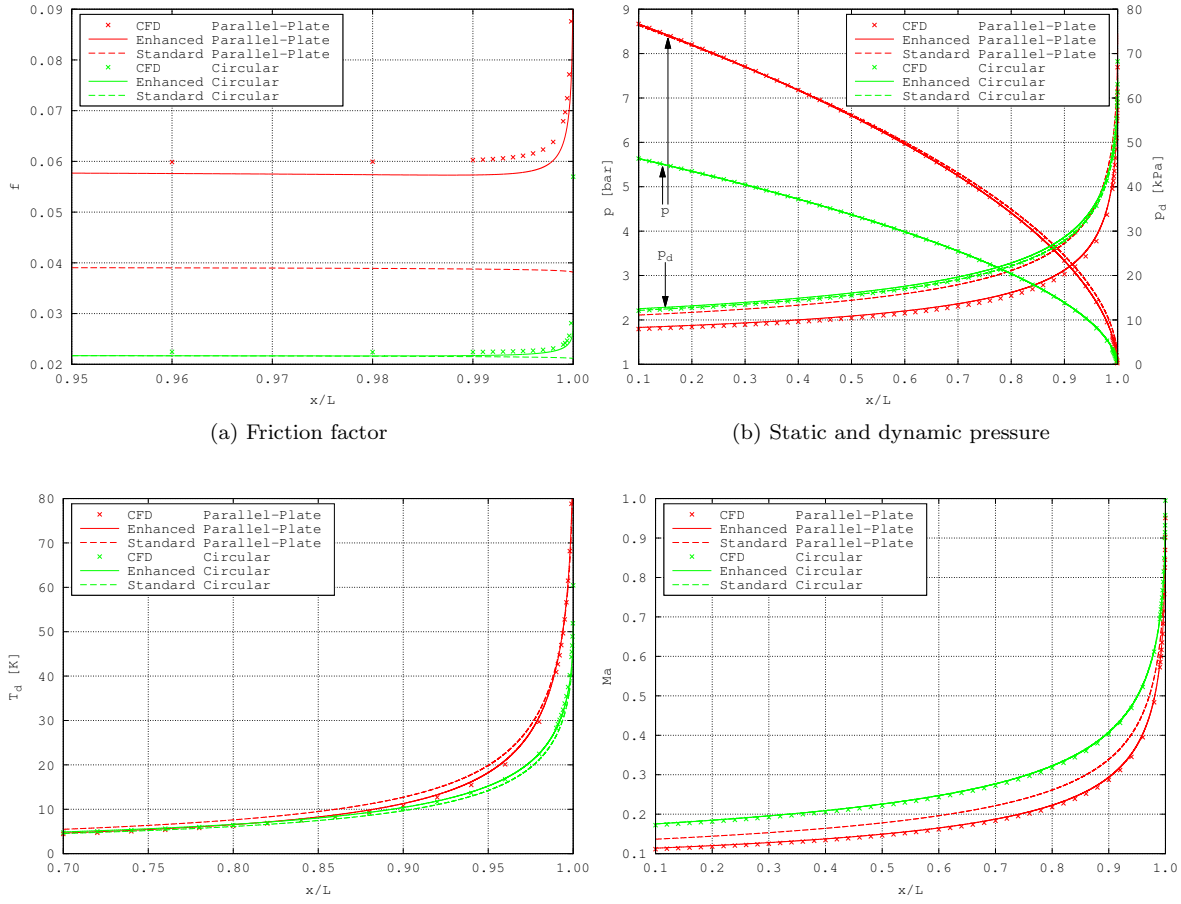

(a) Friction factor

(b) Static and dynamic pressure

(c) Dynamic temperature

(d) Mach number

Figure 8: Model validation: CFD *vs* enhanced and standard one-dimensional Fanno flow model results.

and in Fig. 8c, chosen in order to focus in the region of larger gradients.

The first simulation (parallel-plate cross-section case) shows a much better predicting capability of the enhanced model with respect to the standard one. This is particularly evident for friction factor, but important differences are also found in dynamic pressure and Mach number predictions. As expected, in the second simulation (circular cross-section case) the one-dimensional models are in closer agreements with each other, and differences are evident only for friction factor in proximity of the channel outlet. It is also worth noting the very good agreement between one-dimensional models and CFD results, although Reynolds number is beyond the formal range of validity of the correlations. This confirms the good applicability of the numerical model also in case of large Reynolds numbers, provided that the low-Mach nuber term in Eq. (31) and in Eq. (34) is substituted with the Blasius correlation.

8 Conclusions

An enhanced one-dimensional model for solving turbulent Fanno flow is presented. Compared to the standard models that can be derived from the Fanno theory, the enhanced model implements a series

of CFD calibrated correlations for the accurate evaluation of friction, dynamic pressure, and dynamic temperature at each section. This gives the model a 2D accuracy overcoming the intrinsic limits of the one-dimensional formulation where, out of necessity, every flow-related quantity is represented by a single average value over the section.

The correlations are derived after a detailed analysis of the velocity profiles and their dependency upon Reynolds and Mach numbers due to turbulence and compressibility effects.

The model has been successfully validated also showing the applicability of the correlations proposed outside of the Reynolds number range they are formally calibrated for.

The enhanced model provides an accurate predictive tool for solving compressible turbulent flows in micro-channels. As such it can be used as a fast and accurate micro-channel design tool in real-life applications.

Even though the work is limited to (adiabatic) Fanno flows, its extension to include heat transfer effects should not present particular challenges from the numerical point of view. Considering the nature of the governing equations, it is expected that friction and heat flux will have similar effects on gas compressibility. The choice of adiabatic flow allowed to concentrate only on the effects of friction. The results obtained could also be useful for better separating the effects in possible future works including heat transfer.

References

[1] S.D. Deodhar, H.B. Kothadia, K.N. Iyer, and S.V. Prabhu. Experimental and numerical studies of choked flow through adiabatic and diabatic capillary tubes. *Applied Thermal Engineering*, 90:879–894, 2015.

[2] N. Agrawal and S. Bhattacharyya. Adiabatic capillary tube flow of carbon dioxide in a transcritical heat pump cycle. *International Journal of Energy Research*, 31:1016–1030, 2007.

[3] G.P. Mignot, M.H. Anderson, and M.L. Corradini. Measurement of supercritical CO_2 critical flow: effects of L/D and surface roughness. *Nuclear Engineering and Design*, 239(5):949–955, 2009.

[4] M. Cioffi, E. Puppo, and A. Silingardi. Fanno design of blow-off lines in heavy duty gas turbine. In *Proceedings of ASME Turbo Expo 2013*, San Antonio, Texas, USA, June 3rd-7th 2013.

[5] M. Labois and C. Narayanan. Non-conservative pressure-based compressible formulation for multiphase flows with heat and mass transfer. *International Journal of Multiphase Flow*, 96:24–33, 2017.

[6] H. Grzybowski and R. Mosdorf. Dynamics of pressure drop oscillations during flow boiling inside minichannel. *International Communications in Heat and Mass Transfer*, 95:25–32, 2018.

[7] C. Bao, Z. Jiang, X. Zhang, and J.T.S. Irvine. Analytical solution to heat transfer in compressible laminar flow in a flat minichannel. *International Journal of Heat and Mass Transfer*, 127:975–988, 2018.

[8] P. Rosa, T. G. Karayiannis, and M. W. Collins. Single-phase heat transfer in microchannels: the importance of scaling effects. *Applied Thermal Engineering*, 29:3447–3468, 2009.

[9] Y. Asako, T. Pi, S.E. Turner, and M. Faghri. Effect of compressibility on gaseous flows in microchannels. *International Journal of Heat and Mass Transfer*, 46(16):3041–3050, 2003.

[10] C. Hong, T. Nakamura, Y. Asako, and I. Ueno. Semi-local friction factor of turbulent gas flow through rectangular microchannels. *International Journal of Heat and Mass Transfer*, 98:643–649, 2016.

[11] C. Hong, Y. Asako, G.L. Morini, and D. Rehman. Data reduction of average friction factor of gas flow through adiabatic micro-channels. *International Journal of Heat and Mass Transfer*, 129:427–431, 2019.

[12] S. Murakami and Y. Asako. Local friction factor of compressible laminar or turbulent flow in microtubes. In *Proceedings of 9th ASME International Conference on Nanochannels, Microchannels, and Minichannels, ICNMM 2011*, Edmonton, Alberta, Canada, June 19th-22nd 2011.

[13] M.A. Al-Nimr, V.A. Hammoudeh, M.A. Hamdan, and M.H. Es-Saheb. Fanno flow in microchannels. *Research Journal of Applied Sciences, Engineering and Technology*, 4(24):5578–5585, 2012.

[14] Y. Asako, S.Y. Heng, and C. Hong. On temperature jump condition for turbulent slip flow in a quasi-fully developed region of micro-channel with constant wall temperature. *International Journal of Thermal Sciences*, 136:467–472, 2019.

[15] M. Shams, M.H. Khadem, and S. Hossainpour. Direct simulation of roughness effects on rarefied and compressible flow at slip flow regime. *International Communications in Heat and Mass Transfer*, 36(1):88–95, 2009.

[16] B. Cetin, A.G. Yazicioglu, and S. Kakac. Fluid flow in microtubes with axial conduction including rarefaction and viscous dissipation. *International Communications in Heat and Mass Transfer*, 35(5):535–544, 2008.

[17] O.I. Rovenskaya and G. Croce. Heat transfer in rough microchannels under rarefied flow conditions. *European Journal of Mechanics-B/Fluids*, 72:706–715, 2018.

[18] G.L. Morini. The challenge to measure single-phase convective heat transfer coefficients in microchannels. *Heat Transfer Engineering*, In press, published online on march 15th 2018, 2019.

[19] D. Kawashima and Y. Asako. Data reduction of friction factor of compressible flow in microchannels. *International Journal of Heat and Mass Transfer*, 77:257–261, 2014.

[20] A. Cioncolini, F. Scenini, J. Duff, M. Szolcek, and M. Curioni. Choked cavitation in micro-orifices: an experimental study. *Experimental Thermal and Fluid Science*, 74:49–57, 2016.

[21] J.W. Strutt. Aerial plane waves of finite amplitudes. *Proceedings of the Royal Society of London, Series A*, 84(570):247–284, 1910.

[22] M. Cavazzuti, M.A. Corticelli, and T.G. Karayiannis. Compressible fanno flows in micro-channels: an enhanced quasi-2D numerical model for laminar flows. *Thermal Science and Engineering Progress*, 10:10–26, 2019.

[23] M. Cavazzuti and M.A. Corticelli. Numerical modelling of fanno flows in micro channels: a quasi-static application to air vents for plastic moulding. *Thermal Science and Engineering Progress*, 2:43–56, 2017.

[24] J.D. Anderson. *Modern compressible flow: with historical perspective*. McGraw-Hill, 1990.

[25] P.J. Roache. Quantification of uncertainty in computational fluid dynamics. *Annual Review of Fluid Mechanics*, 29(1):123–160, 1997.

[26] V. Lijo, H.D. Kim, and T. Setoguchi. Effects of choking on flow and heat transfer in micro-channels. *International Journal of Heat and Mass Transfer*, 55(4):701–709, 2012.

[27] P.R.H. Blasius. Das aehnlichkeitsgesetz bei reibungsvorgangen in flüssigkeiten. *Forschungsheft*, 131:1–41, 1913.

[28] C.F. Colebrook and C.M. White. Experiments with fluid friction in roughened pipes. *Proceedings of the Royal Society of London, Series A: Mathematical and Physical Sciences*, 161(906):367–381, 1937.